



---

# **REEL Demo – Romande Energie ELectric network in local balance Demonstrator**

Deliverable: Final depsys report for REeL demo project

Demo site: Chapelle/Rolle

---

Developed by  
Omid Alizadeh-Mousavi  
Sotirios Dimitrakopoulos  
Mahdi Jalali  
Babak Jafarpisheh  
Joël Jatton  
Guillaume Besson  
Antony Pinto  
Simon Reynaud  
Matthieu Junod  
Yann Cheneaux  
DEPSys Sarl

## Table of Contents

1. Introduction.....	2
2. Distribution grid monitoring.....	3
2.1. Rolle.....	3
2.2. Chapelle-sur-Moudon.....	3
3. Data transfer to SCADA .....	7
3.1. Continuous 10-minute interval data transfer .....	7
3.2. Event triggered 10-second interval data transfer.....	8
4. Validation of sensitivity coefficient calculation .....	10
5. LV state estimation with smart meters and GridEye.....	13
5.1. Novelties of the proposed solution .....	13
5.2. Developed state estimation method.....	14
5.3. Results.....	15
6. MV waveform estimation using LV measurement.....	18
6.1. Proposed MV estimation approach.....	18
6.2. Field validation and results.....	20
7. MV topology discovery .....	26
8. LV grid control using flexibilities of grid and home batteries and PV inverters.....	31

# 1. Introduction

This document describes the outcomes of dephys contribution to the REeL demo project from 2016 to 2021. The activities are listed below and described in subsequent sections.

- Distribution grid monitoring in Rolle and Chapelle-sur-Moudon (section 2)
- Data transfer to SCADA of Romande Energie including continuous 10-minute and 10-second event-triggered custom monitoring (section 3)
- Validation of sensitivity coefficient calculation in Chapelle-sur-Moudon (section 4)
- LV grid state estimation with smart meters and GridEye data in Rolle-hospital LV grid (section 5)
- MV waveform estimation using measurement at LV side of MV/LV transformer in Morges (section 6)
- MV grid topology discovery in MV feeders of Puidoux, Chapelle, and Moudon (section 7)
- LV grid control using flexibilities of grid and home batteries, PV inverters, and electric thermal loads in Chapelle-sur-Moudon (section 8)

## 2. Distribution grid monitoring

### 2.1. Rolle

Rolle is an urban distribution grid. At the HV/MV station of Rolle, 2 departing MV feeders and their underlying LV grids are considered as the project’s demo site. The GridEye devices were successfully installed on the LV side of MV/LV transformers in Rolle in 2017. During 2018, GridEye devices were successfully installed at some LV nodes, i.e. street cabinets, in Rolle. In total 62 GridEye devices are installed in the Rolle demo site. Figure 1 shows the geographical locations of the LV grids in which GridEye devices are installed.

The GridEye measurements are used to evaluate the quality of supply across the LV grids in Rolle. The measurement data includes 10-minute values of voltages, currents, active and reactive powers, as well as several power quality indices according to EN50160 such as Total Harmonic Distortion (THD), inverse and homopolar components. This data is primarily used for distribution grid visibility and evaluation of the quality of supply. Furthermore, the data is used by many academic partners to accomplish their activities in different work packages, for instance activities related to demand side management, multi energy grids simulations, and LV grid storage sizing.

The available measurement data from 2017 to Feb-2019 are transferred to the project server in CSV format. During 2019, GridEye API is developed to automatically transfer GridEye measurement data to the project server.



Figure 1. Geographical locations of LV grids in Rolle with installed GridEye devices.

### 2.2. Chapelle-sur-Moudon

The village of Chapelle-sur-Moudon is supplied by 2 MV/LV transformers connected to the same MV feeder. Figure 2 shows these 2 LV grids and the installed GridEye devices.

9 GridEye devices, shown in green, provide measurement data in 10-min basis for depsys activities. These activities include LV grid monitoring, analysis of quality of supply, forecasting of consumption, and LV grid control.

Another 8 GridEye devices installed, shown in red, providing measurement data on a 1-second basis, to support the activities of the project partners on the demand side management, control of soft-open-point, control of batteries. The 1-second data are timestamped voltages, currents, active and reactive powers. An external API is developed to send these measurement data to the project partners, e.g. HEIA-FR, SUPSI, Aurora's grid and previously Commelec.

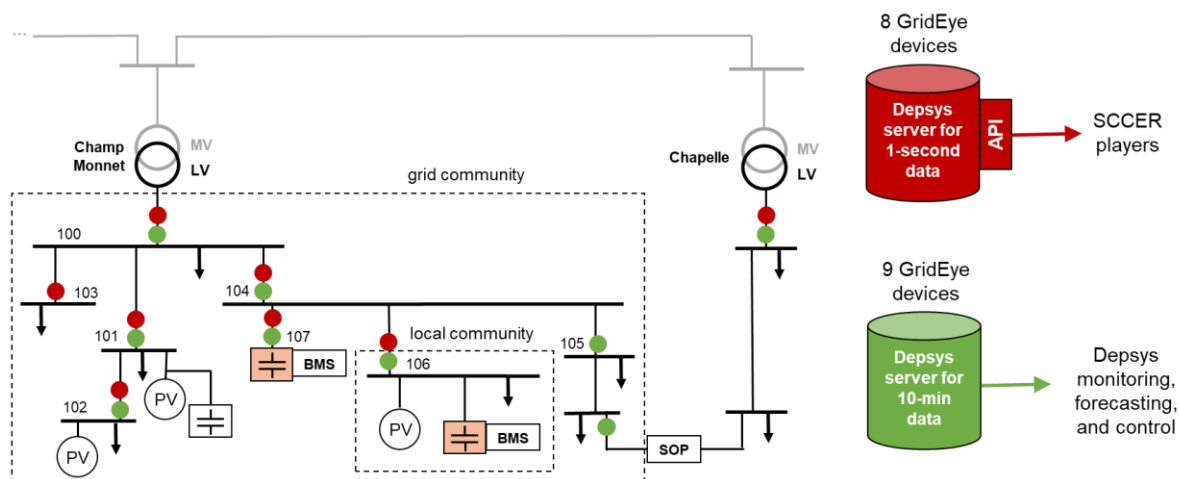


Figure 2. LV grids at Chapelle-sur-Moudon demo site and installed monitoring and control infrastructure.

Figure 3 shows an example of GridEye devices installed in Chapelle-sur-Moudon with different measurement rates (10-min and 1-second).



Figure 3. GridEye devices installed in Chapelle-sur-Moudon with different measurement rates of 10-min and 1-second.

There are more than 300 kWp PV installations in the LV grid of Champ-Monnet. The inverters of a 72 kWp PV installations can be used for LV grid control purposes. The other PV installations are not accessible for the grid control purposes.

A water heating system, including a heat pump of 60kW and 3 electric boilers with the total power of 34kW, is at disposal as a partially flexible electric load which can be

possibly used for grid control purposes. Figure 4 shows the existing controller of the heating system with 4 possibilities of control in the smart grid mode. The descriptions of control modes are given in Table 1, for minimum use of electricity, controlled use of electricity to reach target temperature (default), increased use of electricity, and maximum use of electricity. The target temperatures of the heat pump and the boilers are set to 50°C. Sensors and infrastructure are installed to read the temperatures of 3 boilers and their on/off status. The heat pump controller does not allow reading of the power consumption, and the temperatures of input and output waters. This point can be handled by making some assumptions on the algorithm.

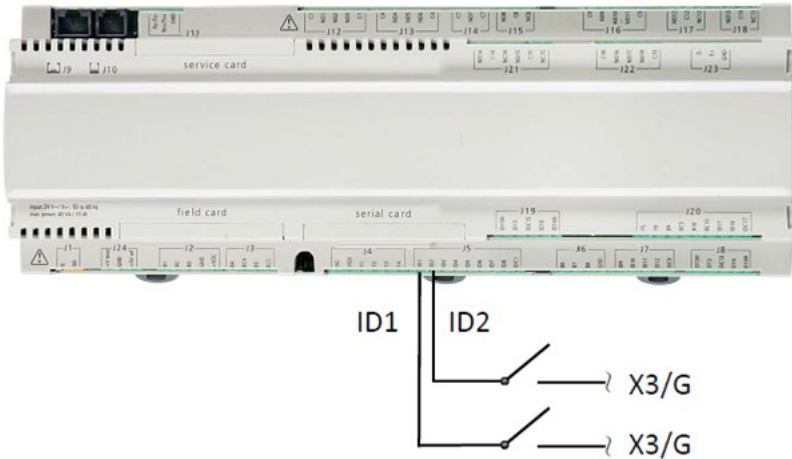


Figure 4. Controller of the heating system with 4 possibilities of control in smart grid mode.

Table 1. Description of heating system control modes.

Color code	ID1	ID2	Description
Red	0	1	Heat the water up to minimum temperature - minimum use of electricity
Yellow (default)	0	0	Heat the water up to target temperature - controlled use of electricity to satisfy the consumption
Light green	1	0	Heat the water up to maximum temperature - increased use of electricity
Dark green	1	1	Heat the water up to maximum temperature, heat pump level 3 and electric heating are activated - maximize use of electricity

The above-described infrastructure is installed in the field. The controller of the heating system is set to the smart grid mode and several tests were done to send control setpoint. However, the controller gives an error message when it is switched to smart grid control mode. After contacting the vendor and manufacturer of the controller, they indicated that the firmware of the controller should be updated but they do not support the firmware update for the existing controller hardware. Thus, the continuation of the activities for the control of heating system requires the replacement of the controller hardware of the heating system. Hence, the heating system control activities are stopped to prevent issues for the continued supply of heated water. The lesson learned is that the complexity of heating systems and their controllers should not be underestimated for the use of their flexibilities. It is worth noting that in the previous project in 2016, depsys had separated 2 boilers (16 kW) from the rest of the heating system and their on/off status (i.e. electricity consumption) was successfully controlled to maximize the

self-consumption considering the available PV production and comfort for the end-customer (i.e. output temperature).

The idea of installing a battery energy storage system for LV grid control and maximization of self-consumption was discussed in 2018 by Romande Energie with dephys and Aurora's grid. GridEye historical monitoring data is used for the optimal sizing of battery storage systems. A grid scale battery storage system (300kWh – 100kW) and a household battery storage system (40kWh – 20kW) were installed at the beginning of 2021. There is another household battery storage system that is privately owned, and it cannot be used as a controllable element in this project.

In addition, the prototype of a soft-open-point (SOP) connecting two LV grids with back-to-back power converters was installed in 2021 for grid control activities.

### 3. Data transfer to SCADA

Two separate mechanisms are developed and put in place to transfer GridEye measurement data to the SCADA system of Romande Energie. The first mechanism continuously transfers GridEye 10-minute measurement data to the SCADA system. The second mechanism transfers GridEye measurement data with 10-second time interval for a period of 5-minutes to the SCADA. The second mechanism is triggered by a rate of change of current. Following sub-sections explain the different steps to realize these mechanisms.

#### 3.1. Continuous 10-minute interval data transfer

A GridEye device is installed in the transformer station of "Corcelles-le-Jorat - Rte du Moulin". This device is connected to the GridEye head-end system present at Romande Energie. The data sent by the device is transmitted to a StreamX concentrator, which is itself connected to the SCADA via the 104 protocol, as shown in Figure 5.

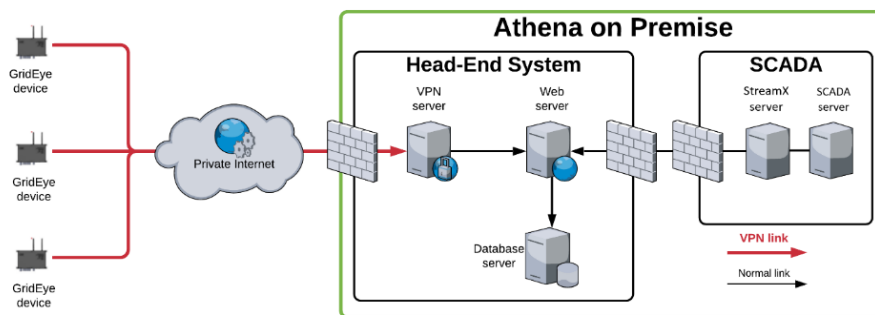


Figure 5. GridEye device data transfer to SCADA system of Romande Energie.

The device installed in Corcelles-le-Jorat is composed of a MCU performing voltage measurements at the LV side, and 3 SURs for current measurements. The first SUR measures the currents of 3 phases and neutral on the LV side. The two other SURs measure the currents of 3 phases on two outgoing feeders at the MV side. Figure 6 shows the installation configuration.

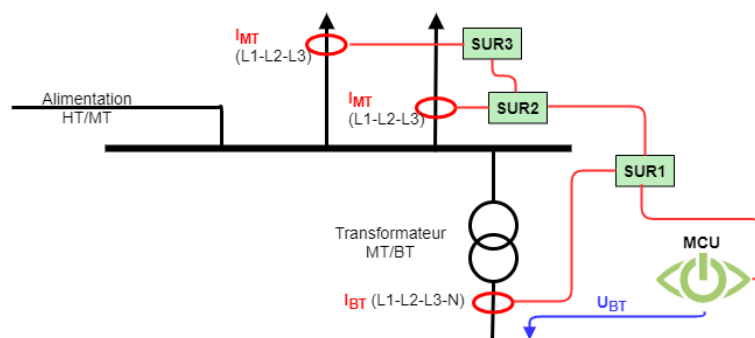


Figure 6. GridEye device installation configuration in Corcelles-le-Jorat.

In order to match the GridEye measurement with the SCADA system of Romande Energie, a data addressing structure is defined in collaboration with Romande Energie.

Each measurement point is composed of a node (corresponding to a voltage measurement) and several inputs and/or outputs (corresponding to current measurements). An ASDU (Application Service Data Unit) is defined for each node and its associated inputs/outputs. Each object contained in an ASDU has an address defined by three bytes, to define the type of measurement carried out. In the pilot phase of the project, the ASDU for each node is assigned manually by depsys. The station in the SCADA of Romande Energie is represented as in Figure 7.

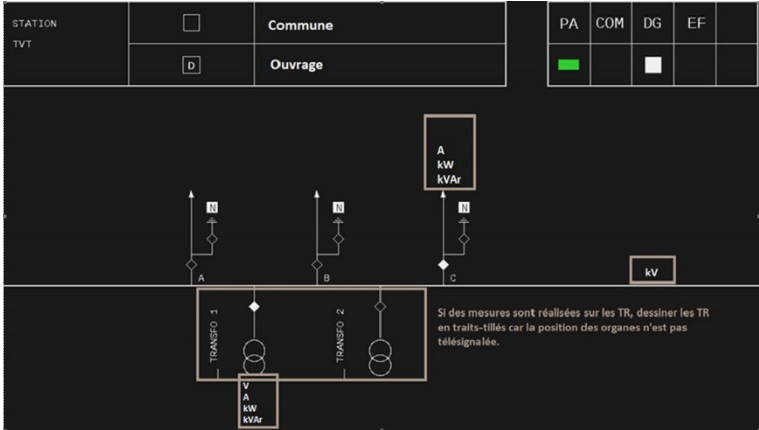


Figure 7. Representation of stations in the SCADA.

The developed solution is deployed to all GridEye devices installed under the HV/MV station of distribution grid in Rolle, as shown in Figure 8. GridEye measurement data integrated in the SCADA system provides Romande Energie with a better visibility of the distribution grid.



Figure 8. GridEye measurements in Rolle are integrated in the SCADA system of Romande Energie providing a better visibility of the distribution grid.

### 3.2. Event triggered 10-second interval data transfer

The continuous data transfer is extended to allow the transmission of 10-second data for a limited time duration. This 10-second interval data transmission is triggered by a current rate of change of  $x$  A/s determined by Romand Energie. In the case of a change

of topology or after an event requiring a voltage restoration, the sudden change of current triggers the sending of 10-second interval data to the SCADA for a duration of 5-minute.

## 4. Validation of sensitivity coefficient calculation

The sensitivity coefficients are used in many power system-related analysis and control approaches. They contain important information on the grid's behaviour and its characteristics. For instance, the voltage sensitivity coefficients reflect the impact of power change at a particular node on the variations of voltage at all nodes. More specifically, the values of the voltage sensitivity coefficients with respect to active power represents the effect of 1 kW additional active power at a node on all nodal voltages within the same grid.

The sensitivity coefficient calculation process is an arithmetic procedure of building a matrix of the partial derivatives. This matrix building process requires a prior power flow analysis, by primarily creating an admittance matrix. The requirements for this are grid topology and parameters, including cable resistance, reactance, and susceptance. The typical approach for the calculation of sensitivity coefficients is through an updated Jacobian matrix. The results of the Jacobian method are considered as the reference for the calculated sensitivity coefficients of other methods.

The model-less approach for determining the sensitivity coefficients only uses the measurement data and does not require the information of grid parameters. The model-less approach is important for determining the sensitivity coefficients in distribution grids for which often an accurate and up-to-date model of the grid is not available.

This work presents the results for the validation of the model-less method for determining sensitivity coefficients of an electric power grid according to which knowledge of the grid parameters is not required and only measurement data are used. The model-less method is studied in the SMILE project, and it is validated in the laboratory environment of the SMILE-FA project. This work presents the results for validation of the estimated sensitivity coefficients using model-less approach with reference to the Jacobian method. The tests are performed using GridEye measurements from the low voltage grid in Chapelle.

Regarding the activities related to the model-less evaluation of the quality of supply in LV grids, the voltage sensitivity coefficients are calculated using three different methods, as described below:

- **Jacobian:** calculation of the sensitivity coefficients using the grid model and the voltages obtained from power flow results. Noting that the power flow results are calculated using the measured nodal power injections. The sensitivity coefficients calculated using the Jacobian method is considered as the reference and they are calculated for every operating point. In this approach it is assumed that the grid model is accurate and up-to-date.
- **Model-less power flow:** calculation of the sensitivity coefficients using the voltages obtained from the power flow results. Reminding that the power flow results are calculated using the measured nodal power injections. Using the "Model-less power flow" method, only one set of the sensitivity coefficients are

calculated for a given duration of measurement data. In this approach it is assumed that an accurate and up-to-date grid model is available.

- **Model-less measurement:** calculation of the sensitivity coefficients using the measured voltages. Using the “Model-less measurement” method, only one set of the sensitivity coefficients are calculated for a given duration of measurement data. The knowledge of the information of grid model is not needed in this approach.

The three methods are used to determine the sensitivity coefficients for the LV grid of Chapelle shown in Figure 9. The calculated voltage sensitivity coefficients using the different methods are presented in Figure 10 where the coefficients are given by  $K_{vp}$  in  $[V/kW]$ . In this grid there are four measurement points, therefore the calculated mutual sensitivity coefficients is a matrix of  $4 \times 4$ , where each row  $i$  and column  $j$  represents the relation between the voltage changes at node  $i$  in  $[V]$  and the power changes at node  $j$  in  $[kW]$ . The outputs of the Jacobian method calculated for every operating point are shown in red. The average value of the Jacobian coefficients is used as the reference for the calculation of  $\pm 10\%$  and  $\pm 50\%$  margins. These margins are shown with the dashed lines. The outputs of the “Model-less power flow” method is given with the blue dashed-dotted line. The outputs of the “Model-less measurement” method, is given with the green line.

Based on these results, the following observations can be made:

- The variation of the Jacobian sensitivity coefficients is around 10%.
- The “Model-less power flow” method is very close to the average value of the Jacobian method by showing an average 4.6% difference. In some cases, the difference between “Model-less power flow” and “Jacobian average value” reaches to around 10% margin.
- The “Model-less measurement” method is also close to the average value of the Jacobian method by showing an average 7.1% difference. In some cases, the difference between “Model-less measurement” and “Jacobian average value” becomes slightly above 10%. Noting that this difference might be due to neglecting the impacts of the fuses/joints/connections impedances and the aging of cables on the grid parameters.



Figure 9. Reduced single line diagram of LV grid of Chapelle-sur-Moudon and location of GridEye devices used for calculation of sensitivity coefficients.

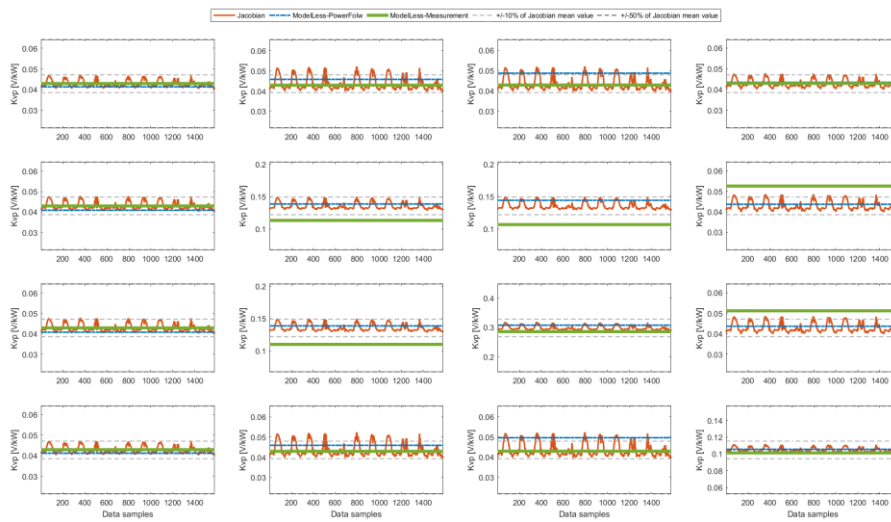


Figure 10. voltage sensitivity coefficients calculated, in red) Jacobian method using grid model, in blue) Model-less power flow method using power flow outputs, in green) Model-less measurement method using field measurements.

## 5. LV state estimation with smart meters and GridEye

The main research question addressed in this work is to make use of existing smart metering data for analysis of low-voltage network. The outcomes of the developed state estimation algorithm for the low-voltage network are evaluated.

This work addresses the applicability of state estimation for cases of aggregated smart meters. The aggregated smart meters can be categorized into two groups: i) aggregated smart meters retaining their original location and ii) aggregated smart meters whose provided locations are different from their original position, which serves to ensure customer's privacy. This procedure does not affect the total energy consumption of the network and is done by the smart meter data provider.

This assessment also provides insights on state estimation under multiple data sources of different timeframes. Finally, the importance of higher-resolution outputs, based on the timeframe of the device of the higher-resolution, is appraised. As such, neglected spikes due to lower-resolution measurements, can be noted numerically and visually.

### 5.1. Novelties of the proposed solution

The importance of state estimation in the operation of the power system led to research in its advancement towards the distribution grids. Currently, there are various state estimation methods. The method of choice depends on the measurement availability, provided data type of measurements and the desired optimization method. The typical method of state estimation consists of a non-linear weighted least-square optimization, where a linearization process is necessary. At this linearized point, a Newton-Raphson procedure produces outcomes, which depend on the pre-set convergence criteria. Thus, the iterative procedure is not only computationally costly, but also potentially non-converging.

This work presents an alternative method for state estimation, where the outcome is produced linearly, without requiring further data inputs than the typical method would require. This is achieved by a reformulation of the states of the network. The optimization is still a weighted least square optimization, but the process becomes a series of matrix multiplications, instead of an iterative single-point solution. Moreover, since the optimization matrix contains network topology and parameters information, it only requires partial update for every timestamp, instead of a new matrix formulation per linearized point for every timestamp.

Moreover, this work sets the basis for acquiring higher-resolution measurements from lower-resolution ones from different measurement device units. Thus, every device can collaborate to produce outputs, based on the outputs of the GridEye device on the transformer level.

The outcomes of this method are validated using field measurements provided by GridEye and smart meter measurements in a low-voltage grid of Rolle.

## 5.2. Developed state estimation method

Power systems are becoming more dynamic and distribution grids will play a bigger role in the future, due to the vital part of distributed generation in the total energy production. This shift is bound to be bigger in the future and adaptations are necessary for all the responsible parties. Thus, energy market-related functions, which are produced typically by the outputs of state estimation algorithms, are gathering more traction.

State estimation provides valuable insights about the network's operating conditions. The produced outputs are typically voltage and current values for all nodes and branches within the network. These outputs are the basis for other functions that operators use, since energy models and network applications outputs are yielded by the products of state estimation.

For the high and medium voltage network, the inputs are usually the SCADA outputs. This is different to the low-voltage one, where the measurement availability is scarce and less accurate. The adaptation towards the low-voltage network requires smart meters.

Originally, state estimation is an iterative process, that tries to minimize the objective function within a linearized point by a Newton-Raphson solver. Developed for the higher voltage network, which contains more measurement units than the LV one, its advantages lie in cases of high measurement redundancy. The non-linear procedure has two inherent problems. First and foremost, the computation time is quite higher than any linear solver. Moreover, convergence is not always ensued for cases where iterations are required.

The developed method relies on reformulation of the states. This reformulation requires more measurements to achieve observability. These additional measurements aid to build a linear reformulated matrix. Nevertheless, by smartly creating assumptions on some of the measurements, the observability conditions are met without requiring additional measurements or imposing any issues in the quality of the outcomes. To achieve this, low weights to the assumed measurement points are induced, that overall do not hinder the algorithm's performance. As mentioned, state estimation operates better with more measurements available, nevertheless, can still produce quality outputs at cases where observability condition is met. The available devices in the network are GridEye devices and smart meters. The collaboration between these measurements is necessary to produce high-quality outputs. GridEye are installed devices at MV/LV transformer and some LV cabinets. These provide quality information every 10 minutes, regarding the voltage, the current and power consumptions per phase. Thus, the balance between the phases is depicted, which is useful for acquiring insight about the smart meter allocation within the network.

Smart meter measurements are also provided, which indicate the location of installation and their energy consumption on a 15-minute time frame basis. The provided consumption is the three-phase consumption. Smart meters are categorized into two different groups, one containing smart meters whose node position is correctly provided and another group, which instead provides aggregated smart meter data at cabinet

positions. For clarification, the aggregated smart meters whose provided location is a cabinet are indicated as 'FDR', while aggregated smart meters who retain their original position are indicated as 'BRP'. This is done to simplify the annotation of the smart meters and to visually comprehend the provided inputs in a graph. This differentiation between the smart meter groups is shown in Figure 11.

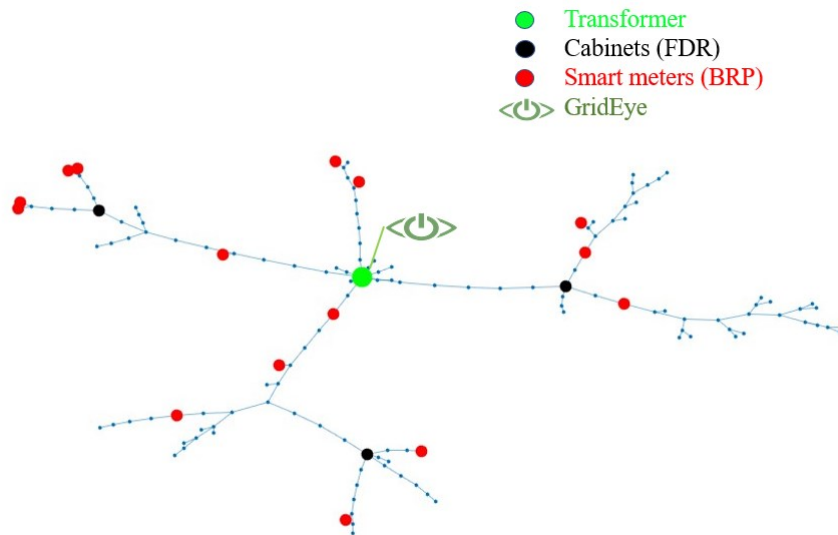


Figure 11. Test case network and positions of various measurement devices.

Since GridEye outputs are higher-quality and resolution than the smart meters, they are vital to the state estimation. GridEye devices constitute the basis for acquiring the smart meter's consumption of active and reactive power per phase. Since smart meter provide energy consumed for the summation of the three phases, GridEye power consumption per phase provide an indication of the per phase consumption, as well as accurate reactive power consumption estimations.

Additionally, this work tackles the issue of multiple timeframes of provided data. Since GridEye measurements and smart meter measurements are provided every 10 and 15 minutes respectively, the common approach would be to run state estimation for the common timeframe of 30 minutes. This work, thus, focuses on acquiring high-resolution 10-minute outputs, by correlating the total of aggregated smart meter inputs to the GridEye device installed on the transformer. This way, smart meters consumptions are not only correlated to the correct phase, but they can be used in the 10-minute window of the GridEye devices. This adaptation provides voltage and current peaks and spikes, which would otherwise be unnoticeable.

### 5.3. Results

The network of the test case is shown in Figure 11. Originally, the network constitutes of 143 nodes. Initially, 176 smart meter devices are installed in the network, distributed within 41 nodes. Since smart meters represent customer consumption, many smart meters can be aggregated to specific nodes. As such, 134 of the smart meters are distributed within 15 nodes as smart meters aggregated at their existing node (BRP). The rest of the smart meters are aggregated in the 3 cabinets and transformer nodes, to ensure privacy of the customers (FDR). These contain aggregated data of smart meters

in different locations, which are aggregated to an artificially created node within the network.

After the reduction process, 27 nodes are fully able to describe the network, in which 18 are nodes of consumption. The reduced network, containing the outcomes of state estimation, is illustrated in Figure 12.

The main outcome of the analysis is the combination of data provided by different measurement systems. The outcomes almost perfectly match the inputs provided in the state estimation (highest error is 0.0016V or 0.0006% for node voltage and 0.02A or 0.017% for branch current). Even when noise is manually introduced based on the levels of trust of the GridEye device, the output error does not exceed the introduced error. The computation time is faster for the linear state estimation compared to the power flow, as typical power flow is iterative.

The outputs of state estimation are visualized in Figure 12, where the branch current with respect to the nominal line current of each line is depicted, as well as the voltage for the nodes. This figure shows the results for one specific timestamp and is used to visualize the outcomes of the method.

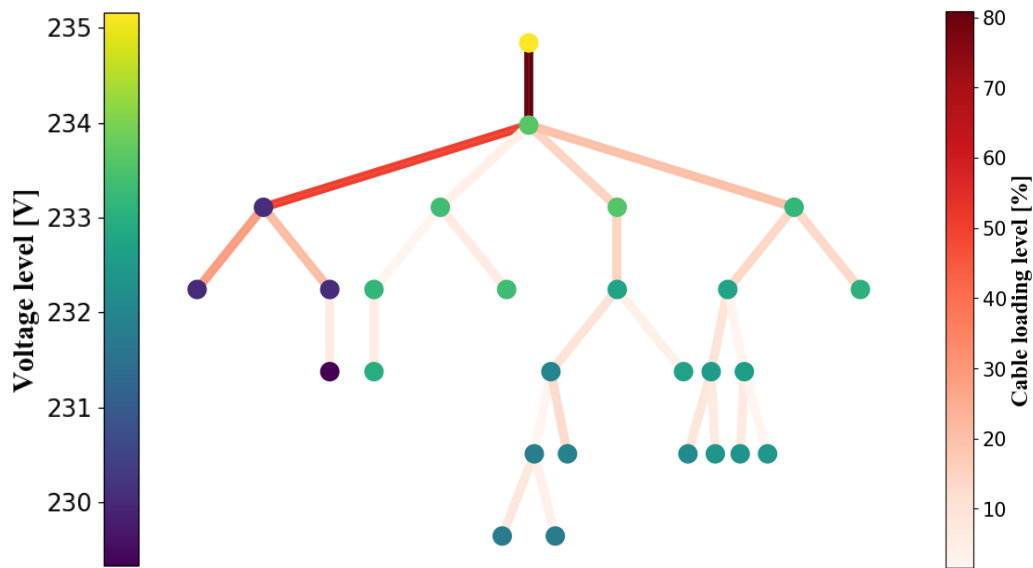


Figure 12. State estimation voltage and current outputs.

Moreover, instead of using only the common-time frames of the measurement devices (every 30 minutes), another goal is to provide deeper insight based on provided measurement data by the GridEye timeframe (10 minutes). By assuming consumed power as a uniform distribution, higher-resolution estimates are achieved. The advantages of higher-resolution state estimation lie in acquiring the network's operating conditions. This can be noted in Figure 13, where the 10-minute state estimation is more insightful, as some voltage and current peaks would be unnoticed otherwise. Figure 13 consists of estimated outputs for one node, which represents several smart meter devices, for both voltage and current.

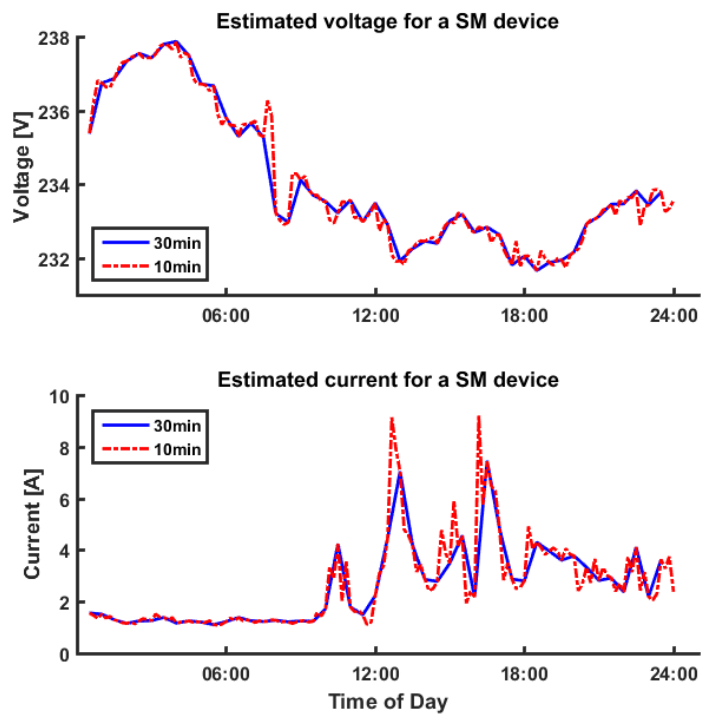


Figure 13. Estimated voltage and current of a smart meter device for different time-resolution within a day.

The results of this deliverable show how to make use of smart metering data along with grid measurements for the analysis of low voltage networks and monitoring of its secure and safe operation.

## 6. MV waveform estimation using LV measurement

This section presents the results of estimating MV voltage and current waveforms using GridEye measurements at the LV side of MV/LV transformer (T/F). The developed method uses discrete time domain equations of a power transformer. Following subsections describe the proposed MV waveform estimation method as well as GridEye installations used for the validation of proposed method. Furthermore, the performance of the proposed method for different sampling frequency is discussed.

### 6.1. Proposed MV estimation approach

The idea of the proposed methodology is based on taking measurements of voltage and current on the low-voltage side of the T/F and, by using the mathematical de-scription of a typical model of single-phase T/F, calculate (as an estimate or projection) what are the values of the voltage and current on the MV side of the T/F. In this sense, the MV side of the T/F is emulated in silico; its digital twin is implemented. As well documented, T/F can be modeled as 2-port systems; either a pi- or a t-equivalent circuit with the resistances, reactances lumped or split, according to the degree of detail sought for (see Figure 13).

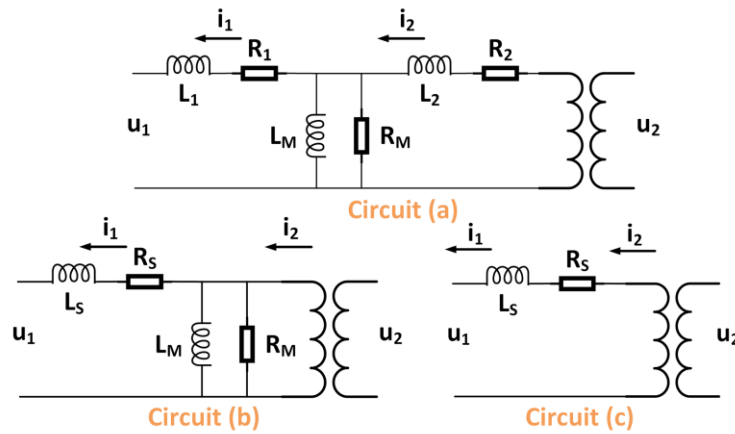


Figure 14. Transformer equivalent models.

Circuit model (a) is the full T/F model, circuit model (b) assumes that all series resistance and reactance is lumped on one side of the T/F as  $R_s=R_1+R_2$  and  $L_s=L_1+L_2$ , while circuit model (c) simplifies (b) by assuming infinite impedance from  $L_m$  and  $R_m$ . Due to its simplicity, circuit model (b) is the preferred digital twin of the MV side of the single-phase T/F for the proposed methodology. Additional detail will only improve the results that follow. As of circuit (b) and assuming that the T/F is sized and operated according to standard (i.e. T/F core saturation is avoided, otherwise a piece-wise formulation may complement the following set-up), the MV calculations are as:

$$\left. \begin{aligned} u_2(t) &= u'_1(t) + R_s i'_1(t) + L_s \frac{di'_1(t)}{dt} \\ i_2(t) &= \frac{u_2(t)}{R_M} + \frac{1}{L_M} \int u_2(t) dt + i'_1(t) \end{aligned} \right\} \quad (1)$$

Where  $u$ ,  $i$ ,  $R$  and  $L$  are voltage, current, resistance and inductance, respectively. Resistances  $R_s$  and  $R_M$  may also be expressed as functions of temperature or of T/F loading (i.e. inferring temperature), to allude to the effect of temperature on resistances at different loads. Voltage and current are given as time variables, since waveforms are measured. Subscripts  $1$ ,  $2$ ,  $S$  and  $M$  denote the LV and MV sides, series and shunt (leakage and magnetizing impedances) parts of the single-phase T/F, respectively. Voltage and current measurements of the LV side are referenced to the MV side (i.e. multiplied by the T/F ratio). Any tap-changing action in the T/F is considered an input to the digital twin model. Alternatively, tap-changing can be monitored electrically by the digital twin and, thus, adjust values in (1). Let it be stressed that (1) may also calculate any harmonics content either in the voltage or the current of the MV-side of the T/F, provided it is present in the LV-side measurements. The only concern with regards to this calculation stems from any filtering effects probably caused by the T/F impedance.

For the digital twin of a three-phase T/F, the approach builds on that of the single-phase as follows: the digital twins of three single-phase T/F, each taking separate single-phase voltage and current measurements from the LV side of a three-phase T/F, are appropriately integrated to emulate the three-phase voltage and current of the MV side of the T/F. Practically, voltage and current measurements of each phase on the LV side are used to calculate the corresponding values of one of the phases on the MV side through (2). The overall digital twin topology is shown in Figure 15. Following, the calculated values are elaborated according to the vector group of the T/F; i.e. the connection of the three phase windings. For the most commonly T/F vector groups in distribution systems, the phase voltages and the line currents of the MV side for one of the phases are as follows:

$$\mathbf{Yy0}: u_A = u_{2A} \text{ and } i_A = i_{2A} \quad (3)$$

$$\mathbf{Dy1}: u_{AB} \cdot \sqrt{3} = u_{2A} - u_{2C} \text{ and } i_A = i_{2A} - i_{2C} \quad (4)$$

$$\mathbf{Dy11}: u_{AB} \cdot \sqrt{3} = u_{2A} - u_{2B} \text{ and } i_A = i_{2A} - i_{2B} \quad (5)$$

Where subscripts  $A$ ,  $B$ ,  $C$  denote the three phases of the MV side of the digital twin of the three-phase T/F, and subscript  $2X$  (where  $X = A, B, C$ ) denotes the calculated values of the single phase MV side digital twin from LV measurements via (2). Grounding either T/F side does not alter formulations (3-5). The digital twin of a T/F connected as Dy will not be able to calculate MV-side current harmonics of orders multiples of the third, since such T/F topologies eliminate said harmonics.

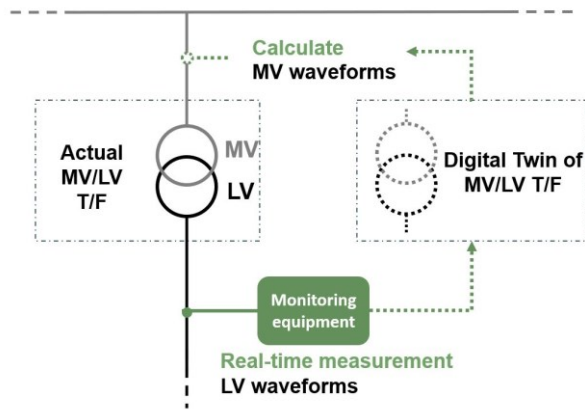


Figure 15. overall schematic of transformer digital twin.

The accuracy of the estimated values are evaluated in terms of normalized root mean square error (NRMSE), given in following equation:

$$NRMSE = \sqrt{\frac{\sum_{n=1:N} (x_n - \hat{x}_n)^2}{N \cdot x_{rms}^2}} \quad (5)$$

## 6.2. Field validation and results

The proposed MV waveform estimation method is tested using two GridEye devices installed in an auxiliary substation in Morges as shown in Figure 16. The MV waveforms are calculated using the waveform measurements of GridEye device installed at the LV side, and then the calculated values are compared with the waveforms measured by GridEye device installed at the MV side. It should be noted that the waveform measurements of these two GridEye devices are time-synchronized with the precision of 19us.

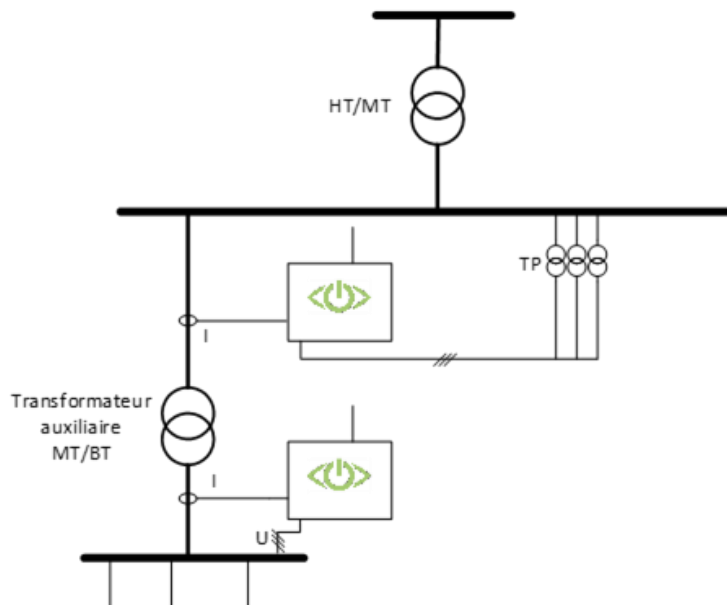


Figure 16. Installation of GridEye devices in Morges for validation of MV waveform estimation.

Several synchronized waveforms were recorded in 2017 and in 2021. Figure 17 shows the estimated MV voltages in solid lines and the measured MV voltages in dotted lines. The figures at the top and bottom are the results of the recordings in 2017 and 2021, respectively. The mean voltage error between the estimated and measured waveform is less than 2%.

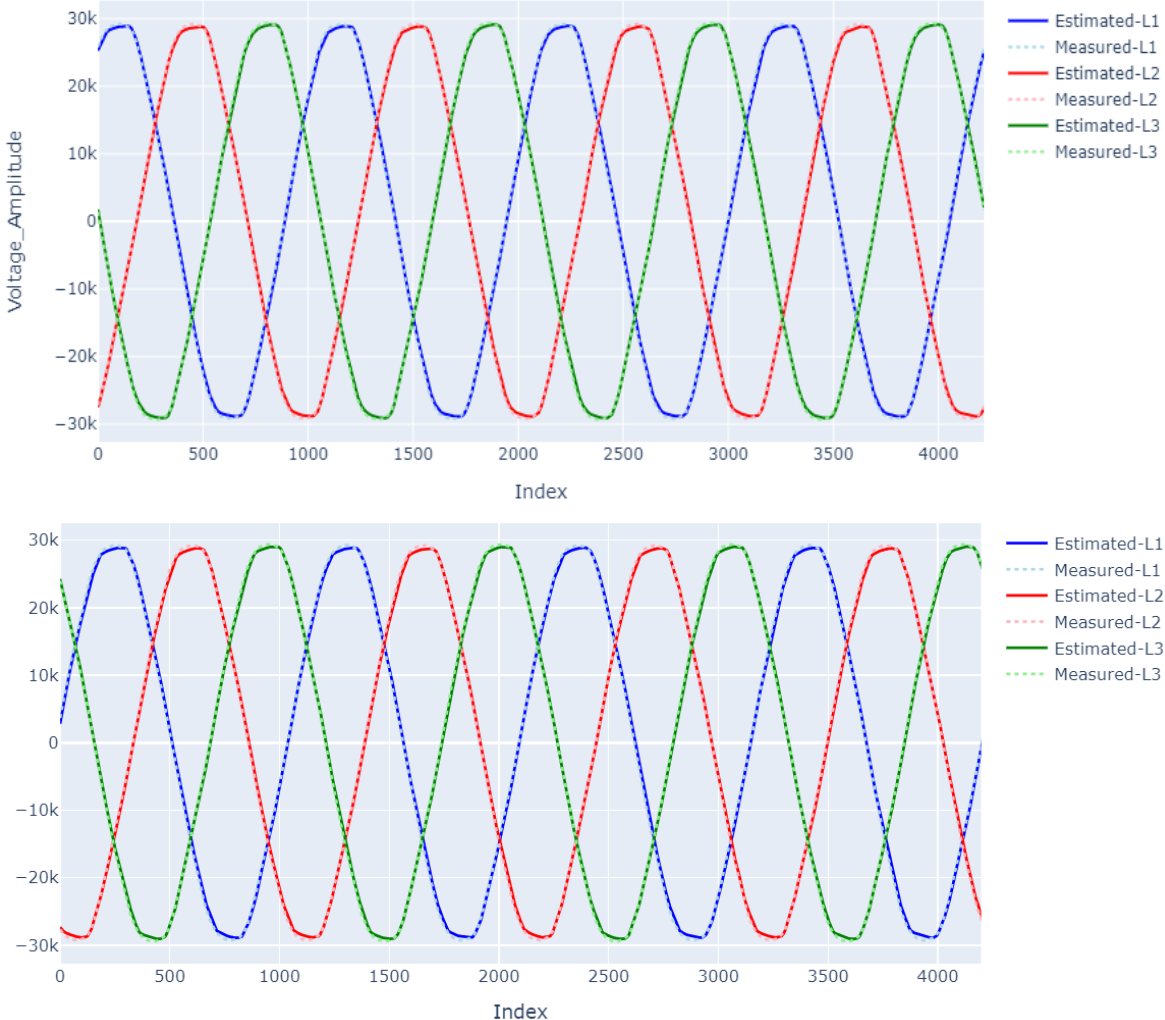


Figure 17. Estimated and measured MV voltages; **top**) recorded waveforms in 2017, and **bottom**) recorded waveforms in 2021

Figure 18 shows the estimated MV currents in solid lines and the measured MV currents in dotted lines. The figures in the top and bottom are the results of the recordings in 2017 and 2021, respectively. The mean current error between the estimated and measured waveform is less than 3%. Note that the measured MV currents are less than 10Arms which is relatively low for the used current sensors.

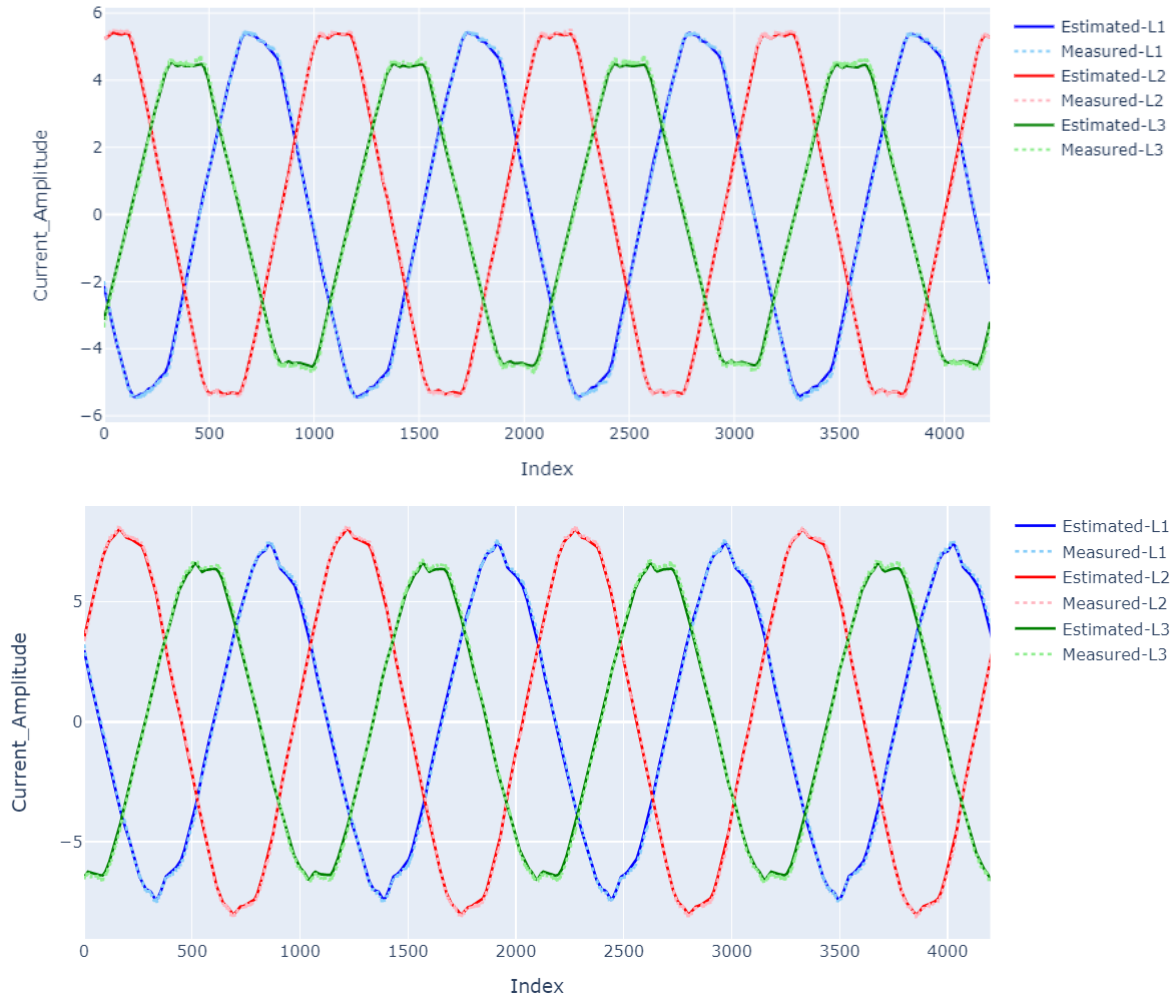


Figure 18. Estimated and measured MV currents; top) recorded waveforms in 2017, and bottom) recorded waveforms in 2021

Figure 19 shows the frequency domain analysis of the estimated MV voltages in dark color and the measured MV voltages in light color. The figures in the top and bottom are the results of the recordings in 2017 and 2021, respectively. The mean voltage error at the fundamental frequency is 0.7% and the mean THD error is 5%.



Figure 19. Frequency analysis of the estimated and measured MV voltages; **top)** recorded waveforms in 2017, and **bottom)** recorded waveforms in 2021

Figure 20 shows the frequency domain analysis of the estimated MV currents in dark color and the measured MV currents in light color. The figures in the top and bottom are the results of the recordings in 2017 and 2021, respectively. The mean current error at the fundamental frequency is 1% and the mean THD error is less than 8%.

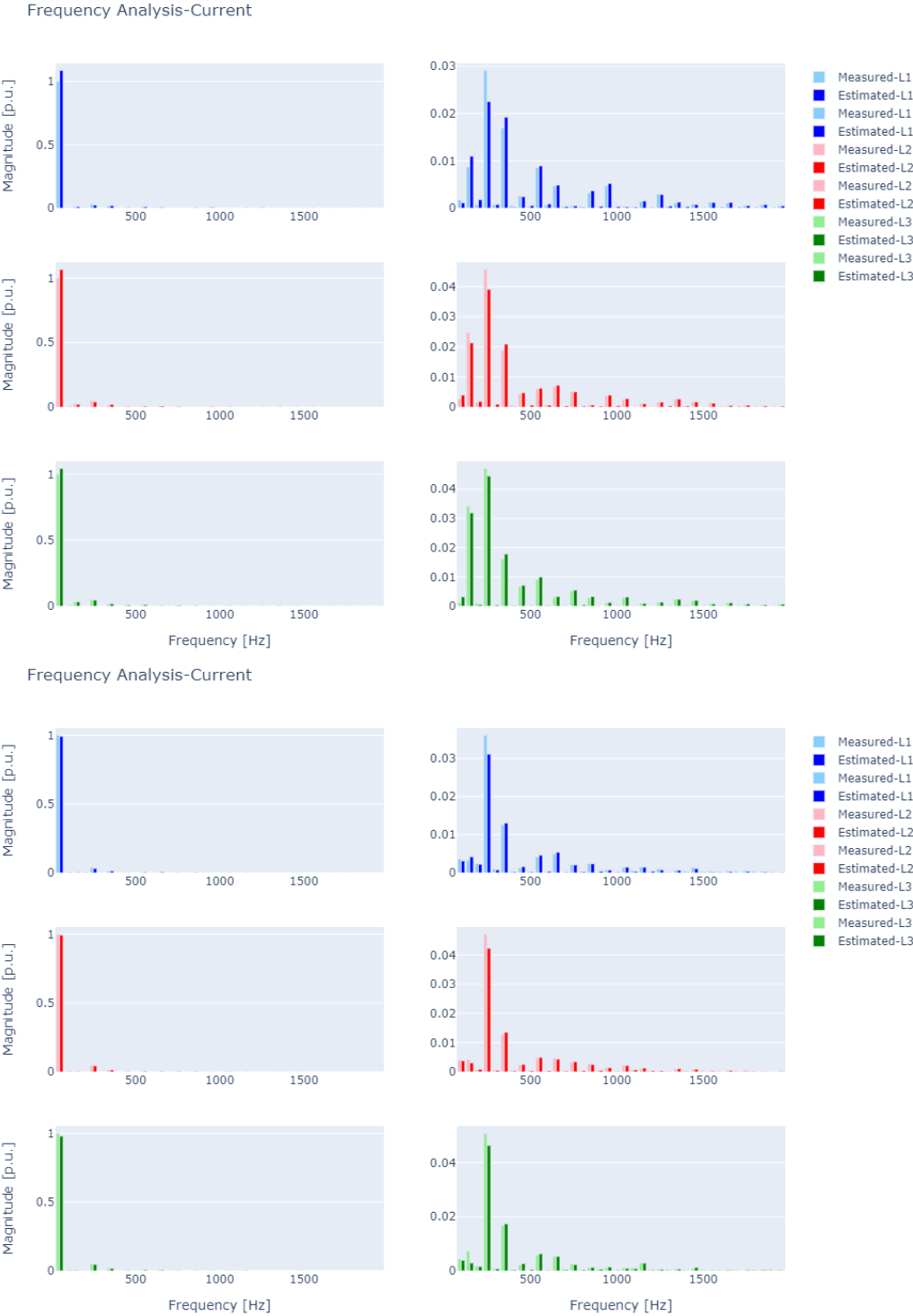


Figure 20. Frequency analysis of the estimated and measured MV currents; **top**) recorded waveforms in 2017, and **bottom**). recorded waveforms in 2021

The main contributions of this work are as follows:

- Monitoring distribution systems at high time granularity is made possible by the digital twin of transformer,
- The waveform monitoring allows to determine power quality at MV and LV, as it captures all harmonics content,
- MV DS behavior under faults can be captured fully to alert the system operator and logged for further analysis, and
- The MV-side waveforms outputted by the digital twin of the T/F are as accurate as the measurements of an instrument T/F on the MV side of the actual T/F.

The developed digital twin model of transformer provides following advantages

- Technical personnel and system operator can assess immediately any remedial actions to system events,
- The cost of measurement instrumentation at the LV side of a power T/F is considerably lower than that of the MV side or of monitoring both sides, thus, making the method less costly for system operators with multiple feeders to cover, and

Installation of LV side measurement devices requires the MV network to be interrupted under fewer circumstances, thus, enabling a comparably seamless deployment. The testing results show that the digital twin properly calculates all line-to-line voltage and current waveforms on the MV side of the DS T/F. However, the method fails in accurately calculating the phase voltages of the MV side of the DS T/F in the following cases:

- the fault is line-to-line-to-ground (LLG) or LG and
- the T/F is connected as Dy (regardless of grounding) or Yy with only one or neither of the two sides grounded and
- the upstream (in the grid) substation is grounded at its MV side.

## 7. MV topology discovery

The objective of this work is identification of MV grid topology using GridEye measurements. In other words, we determine every installed GridEye at LV side of MV/LV transformers is connected to which HV/MV substation. In this project, the MV topology identification is studied for the MV nodes with installed GridEye that are located between the feeders of Moudon (56), Chapelle (51, 53, 54), and Puidoux (57, 58) HV/MV substations, as shown in Figure 21. The existing GridEye devices installed at the LV side of MV/LV transformers along these MV feeders are used for the validation of topology discovery algorithms. In addition, new GridEye devices are installed at the HV/MV substations measuring MV voltage, as shown in Figure 22, either using auxiliary MV/LV transformers (possibility 1) or via existing voltage transformers (possibility 2).

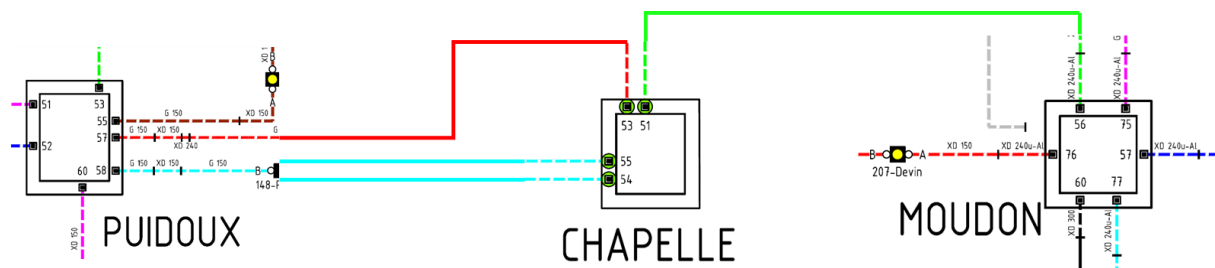


Figure 21. schematic of HV/MV substations and MV feeders connecting them used for MV grid topology discovery.

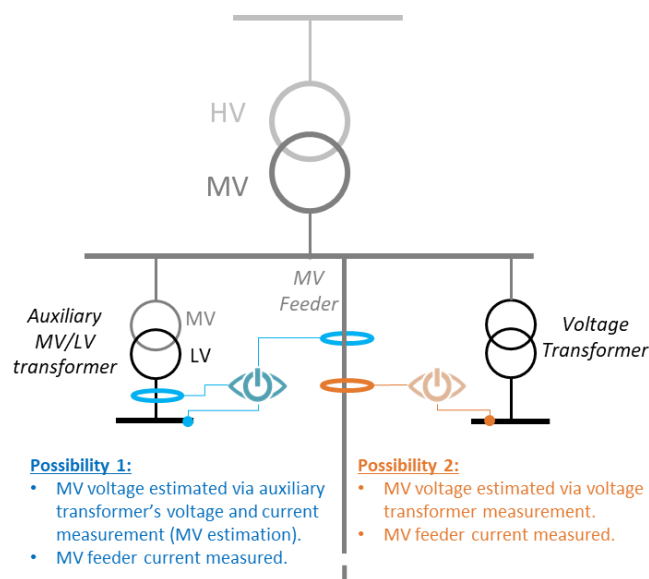


Figure 22. Schematic of two possibilities for MV voltage and current measurement at HV/MV transformer.

Figure 23 shows the schematic of MV grid and HV/MV substations and installed GridEye devices at the substations (green: Moudon, blue: Puidoux, red: Chapelle) and other devices (in grey) at the LV side of MV/LV transformers along the MV feeders. Every MV feeder is supplied only by one of the HV/MV substations (Moudon, Chapelle, Puidoux).

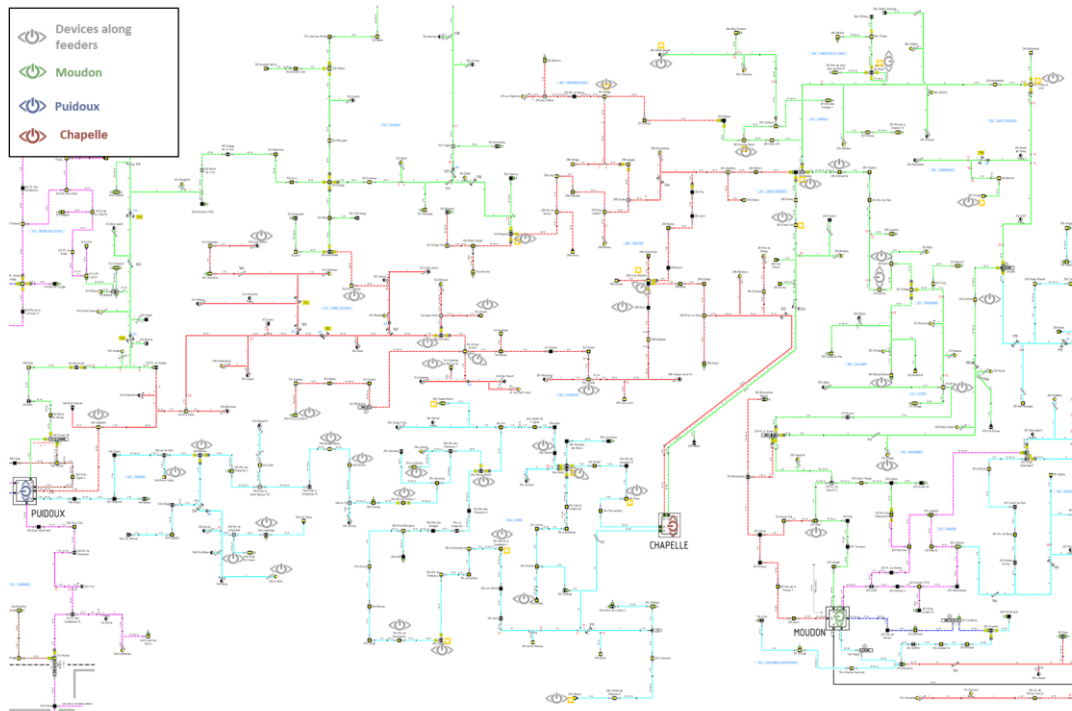


Figure 23. Schematic of MV grid and HV/MV substations and installed GridEye devices at the substations (green: Moudon, blue: Puidoux, red: Chapelle) and other devices (in grey) along the MV feeders.

The inputs of the developed algorithms are i) three phases voltage measurements, ii) name of devices measuring HV/MV substation, iii) vector group of transformers. At first, all GridEye devices perform a synchronized data acquisition of TRMS voltages with 100-milliseconds granularity for a duration of 5-minutes. At the second step, the phase-to-ground voltage measurements are transformed to line-to-line voltage values at MV side, considering the vector group of MV/LV transformers. At the third step, the line-to-line voltage values are averaged over 1 second. Then, at the fourth step, the data is normalized between 0 and 1. In fifth step, the temporal variation of the normalized data is calculated by differentiating data of two consecutive time stamps, from now on called normalized voltage variation. At the last step, a multi-linear regression is performed on the normalized voltage variations of every GridEye along the feeder ( $y$ ) and 3 GridEye devices at the HV/MV substations ( $x_1, x_2, x_3$ ). The largest calculated regression coefficient indicates that the HV/MV substation to which a GridEye device is connected to.

The algorithm is tested at two instances on 30.09.2021 (the summer topology) and on 03.12.2021 (the winter topology). The results of the topology discovery algorithms for the summer and winter topologies are presented in Figure 24 and Figure 25, respectively. The identified topologies are validated with the snapshots of the SCADA system of Romande Energie. The identified topologies at summer and winter modes perfectly match with the snapshots of SCADA, shown in

Figure 26 and Figure 27. Figure 24 shows that at the summer mode, all the feeders are supplied by HV/MV substations in Puidoux and Moudon and the HV/MV substations of Chapelle does not supply any feeder. In winter mode, all three HV/MV substations are used to supply the feeders.

The developed algorithm in this section allows identifying MV grid topology in less than a few minutes. This information can be used to determine the open/close status of switches. The up-to-date and accurate information of grid topology is important for the secure grid operation and taking decisions for optimal grid operation.

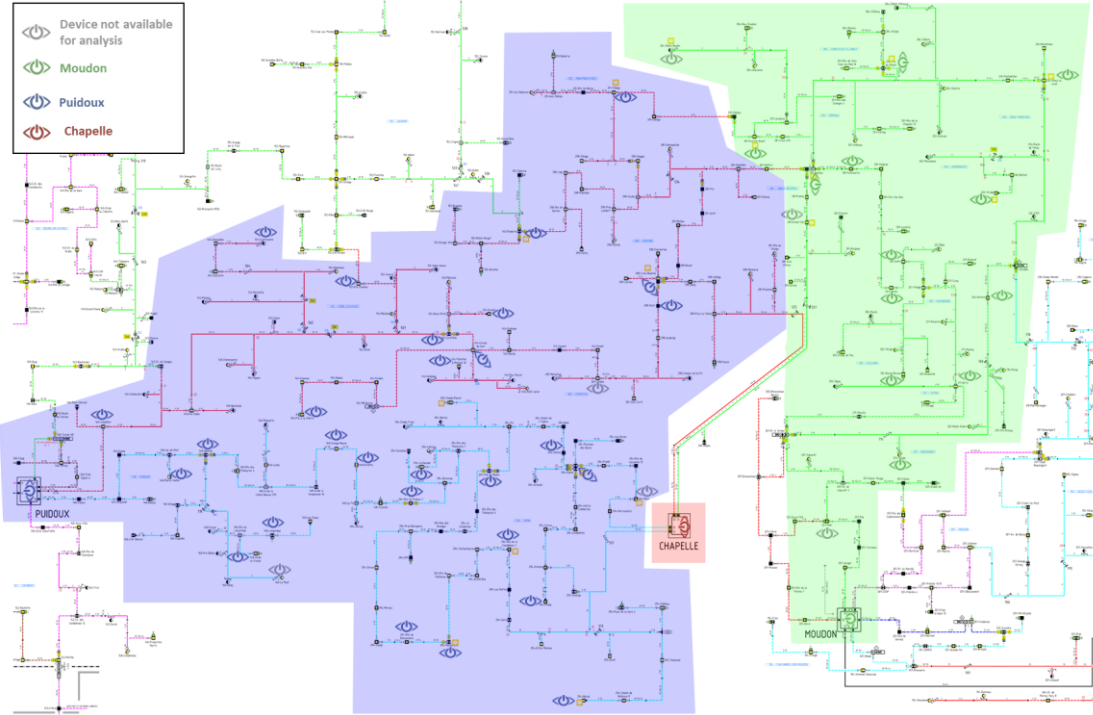


Figure 24. Identified summer mode topology on 30.09.2021

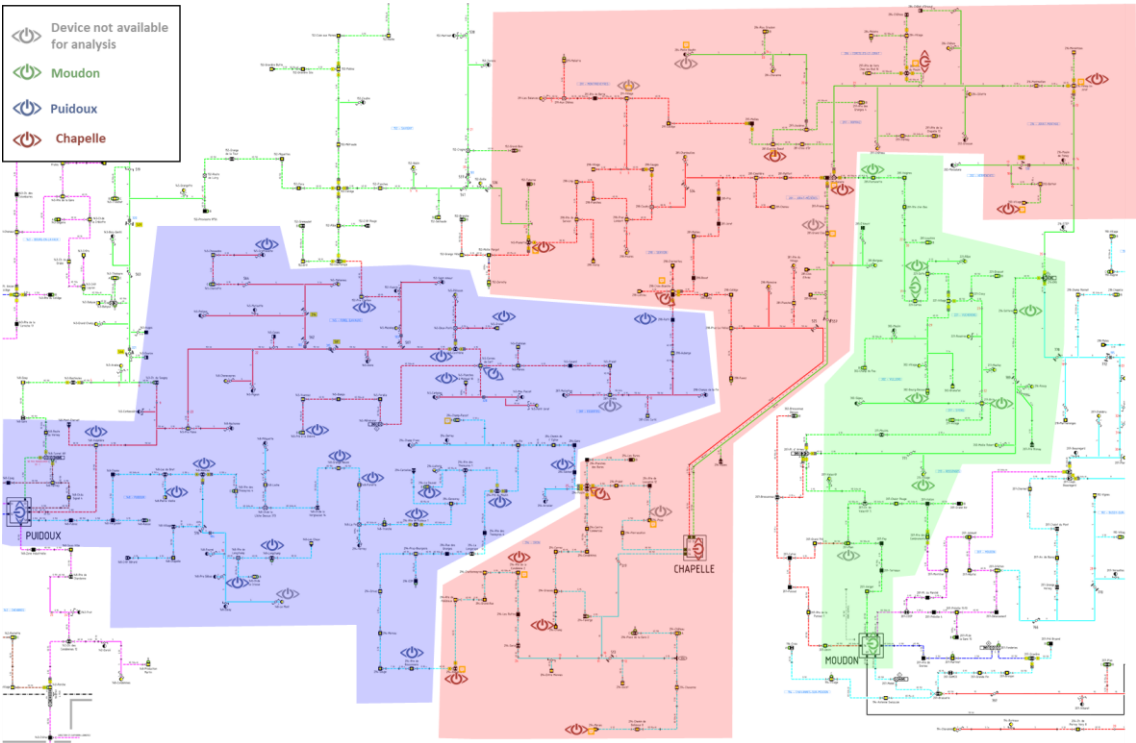


Figure 25. Identified winter mode topology on 03.12.2021

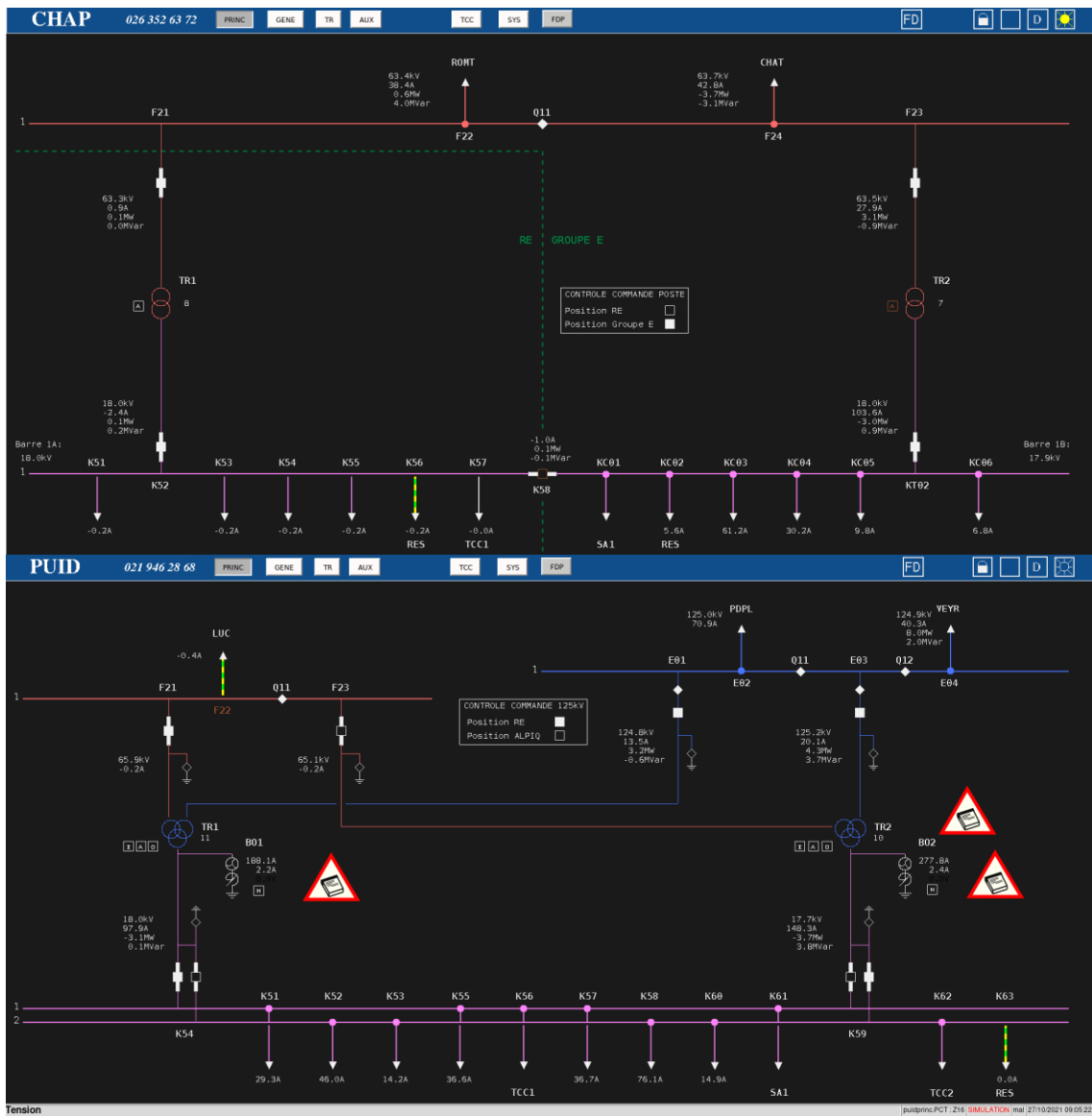


Figure 26. SCADA screen shots on 30.09.2021.

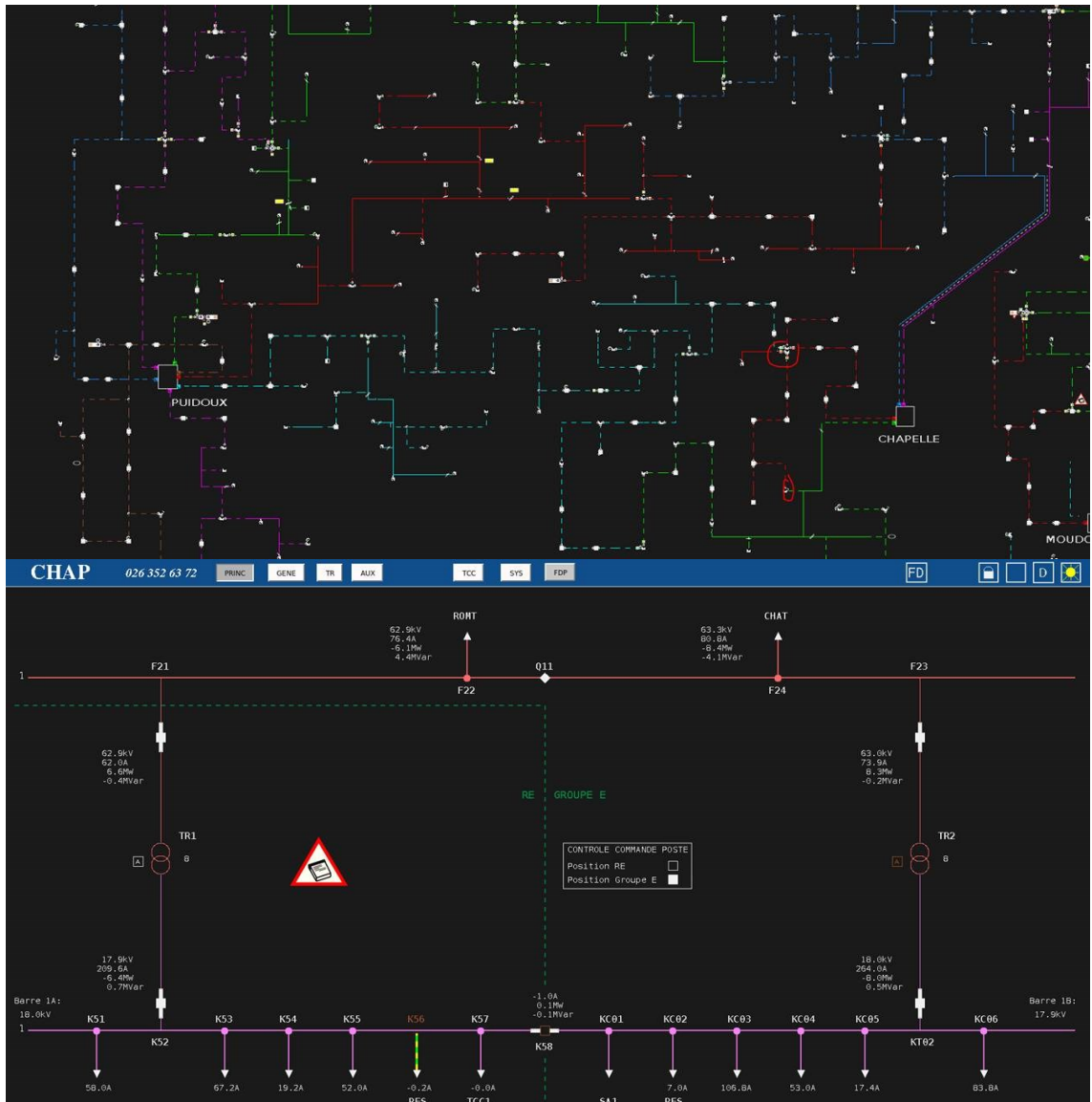


Figure 27. SCADA screen shots on 03.12.2021.

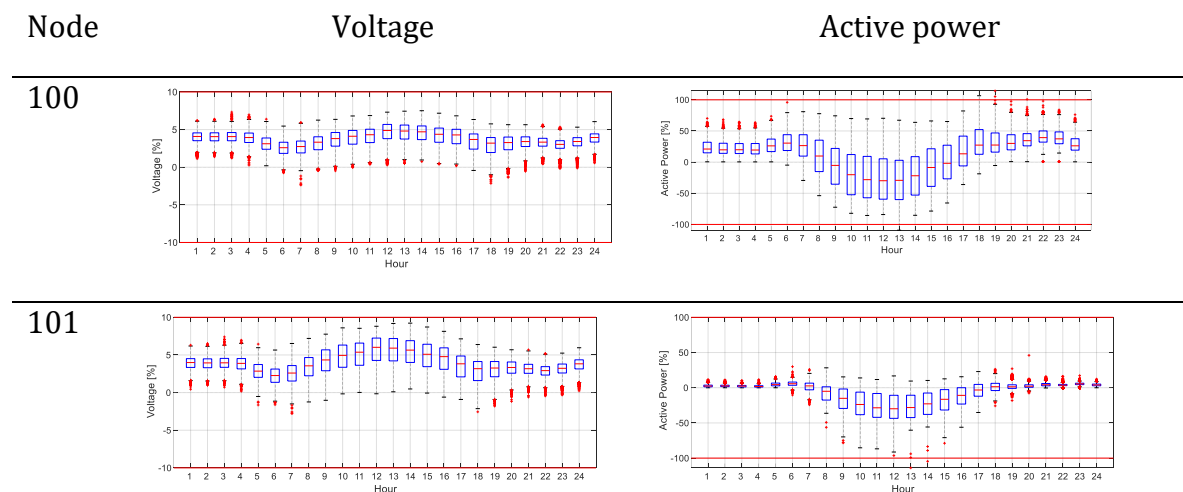
## 8. LV grid control using flexibilities of grid and home batteries and PV inverters

The installed GridEye devices in LV grid of Chapelle-sur-Moudon, shown in Figure 28, providing measurement data every 10-minutes, are used for evaluation of the quality of supply with respect to the grid operation standards, in terms of voltage levels and power flow limits. The data can be used also for grid planning analysis and integration of new production and consumption at each node based on the existing grid situation and remaining margins to the limits of voltage and congestion. Moreover, the historical measurement data are used for battery energy storage sizing and evaluating the impacts of the battery on the self-consumption, peak reduction, and voltage control.

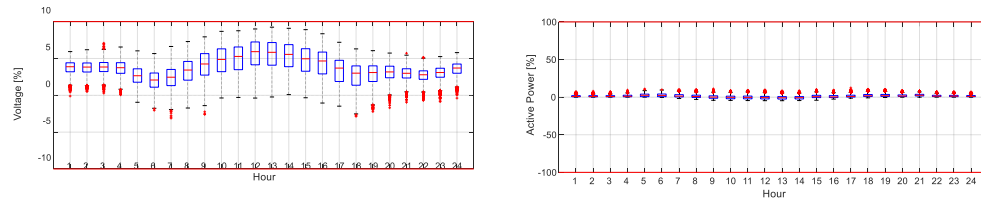


Figure 28. Reduced single line diagram of LV grid of Chapelle-sur-Moudon and location of GridEye devices used for grid analysis.

The hourly statistics of the monitored nodes of the grid for voltages and active powers are shown in Figure 29. The statistics show that PV production has a significant impact on the grid, resulting in high voltage values close to the maximum acceptable level (i.e. 230V +10%) specifically at nodes 101 and 102. Moreover, the transformer loading (i.e. node 100) reaches to its nominal capacity in production (i.e. negative active power) and consumption (i.e. positive active power) for a limited duration.



102



104

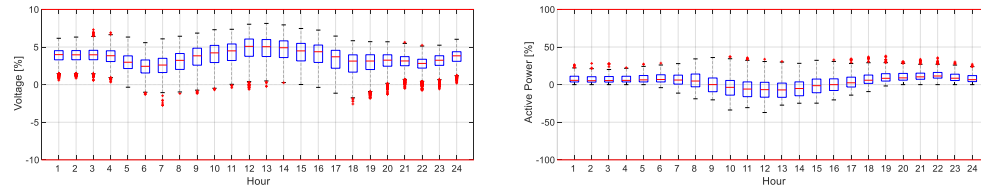


Figure 29. Hourly statistics of voltages at monitored node and in-feeding active power of those nodes in Chappelle-sur-Moudon.

The voltages close to the maximum acceptable limits and overloading for short duration implies the need for the management of voltages and congestion. A primary solution can be the grid reinforcement by replacing the existing transformer (250 kVA) with a larger transformer and also reinforcing some of the cables. An alternative, cheaper and faster, solution is the use of distributed flexibilities for management of power flows and voltage levels. The alternative solution requires the use of grid real-time monitoring device, control and communication interfaces, access to local flexibility resources, and optimization and management algorithms.

The available flexibility resources in the LV grid of Chappelle-sur-Moudon are listed below:

- A grid scale battery storage system (300kWh – 100kW) and a household battery storage system (40kWh – 20kW). These batteries were installed in the beginning of 2021. There is another household battery storage system that is not controllable in this project.
- PV inverter of 72 kWp. There are other PV installations in this LV grid that cannot be accessed for the grid control.

The developed algorithms use the GridEye’s measurements data for forecasting of loads and generations, then evaluating the voltages and power flows, and finally determining the optimal set-points of the flexible resources.

At the first stage, the developed algorithms are applied on the battery storage systems. The objectives of control are maximization of self-consumption at the transformer level and at the local community level. It should be noted that the batteries are allowed to be charged if PV production is larger than the consumption. In other words, the batteries should not be charged from the upstream grid.

Figure 30 shows the single line diagram of the grid, the battery storage systems, the GridEye monitoring devices sending their data to dephys server, and dephys control server calculating and sending control set-points to the batteries. Note that the access to read the state-of-charge of batteries and write active power set-points on them is provided by another company.

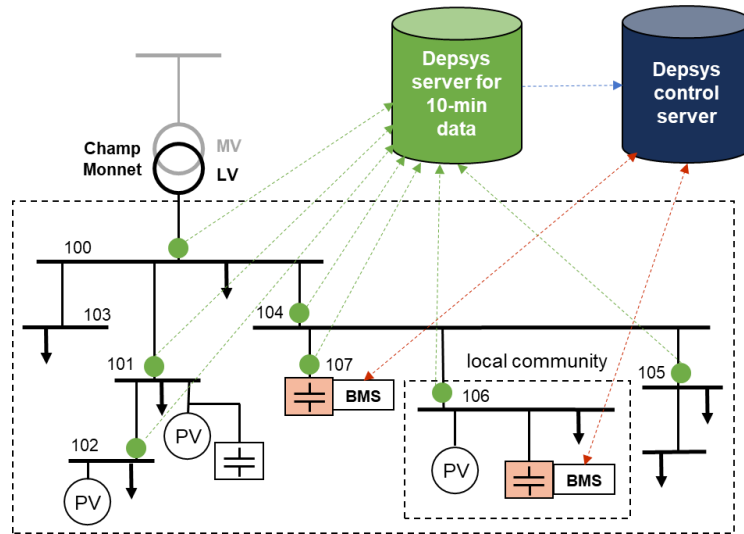


Figure 30. Use of real-time grid monitoring data for control of batteries in Chapelle-sur-Moudon.

The results of the implementation of the proposed control mechanism for a week (2021/09/07 00:00:00 - 2021/09/14 23:50:00) are reported. To assess the accuracy of the real-time control mechanism, the results are compared with the optimal values calculated by the actual data, called after-the-fact analysis. In the after-the-fact analysis, it is supposed that the actual net-load for the entire time horizon is known. The real-time forecasts in comparison with the actual measurement is shown in Figure 31. Figure 31 shows that the application of updated real-time grid monitoring data without weather-based features can predict the net-load pattern accurately even for the days with high volatility in PVs' generation, e.g. 11-12 September. The accuracy of the proposed forecasting method in terms of 10-minutes ahead and peak load forecasting are 2.4% and 4.1%, respectively. The proposed forecasting method has successful performance for both sunny and cloudy days.

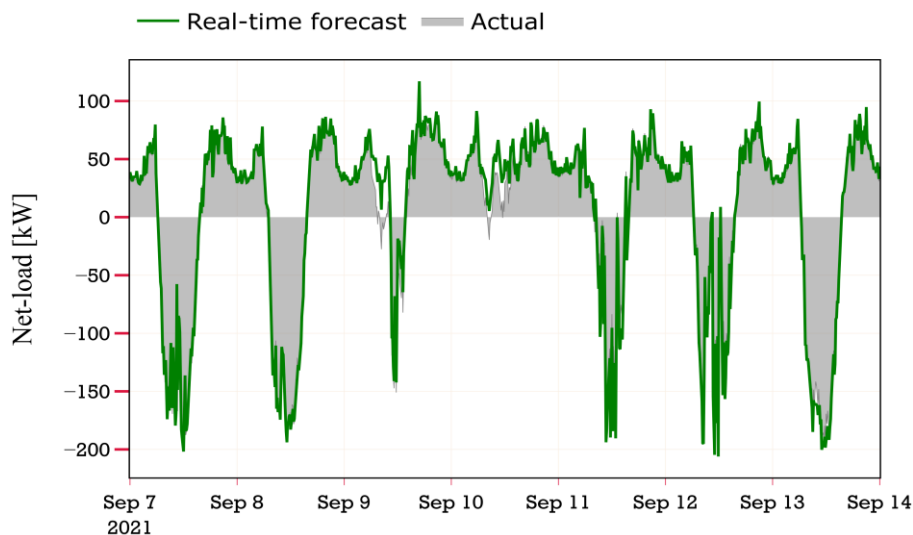


Figure 31. Real-time forecast and actual net-load.

The results of the real-time optimal control mechanism for the real LV grid are discussed. The performance of the determined optimal set-points using the real-time control

scheme are evaluated with respect to the after-the-fact results, as shown in Figure 32. The after-the-fact results are calculated using the actual values of the net-load in the next 24-hours, thus they are considered as the ideal solution in which there is no forecast error. The differences between the charging and discharging regimes of the batteries in the real-time schedule and the after-the-fact analysis are caused by the forecasts errors of the next 24-hours. The real-time method traces efficiently the after-the-fact scheduling. According to the forecasted net-load (see Figure 31) and the determined charging/discharging powers of the batteries (see Figure 32), it is concluded that the batteries are charged when there is surplus PV production, and they are discharged when the net-load is positive.

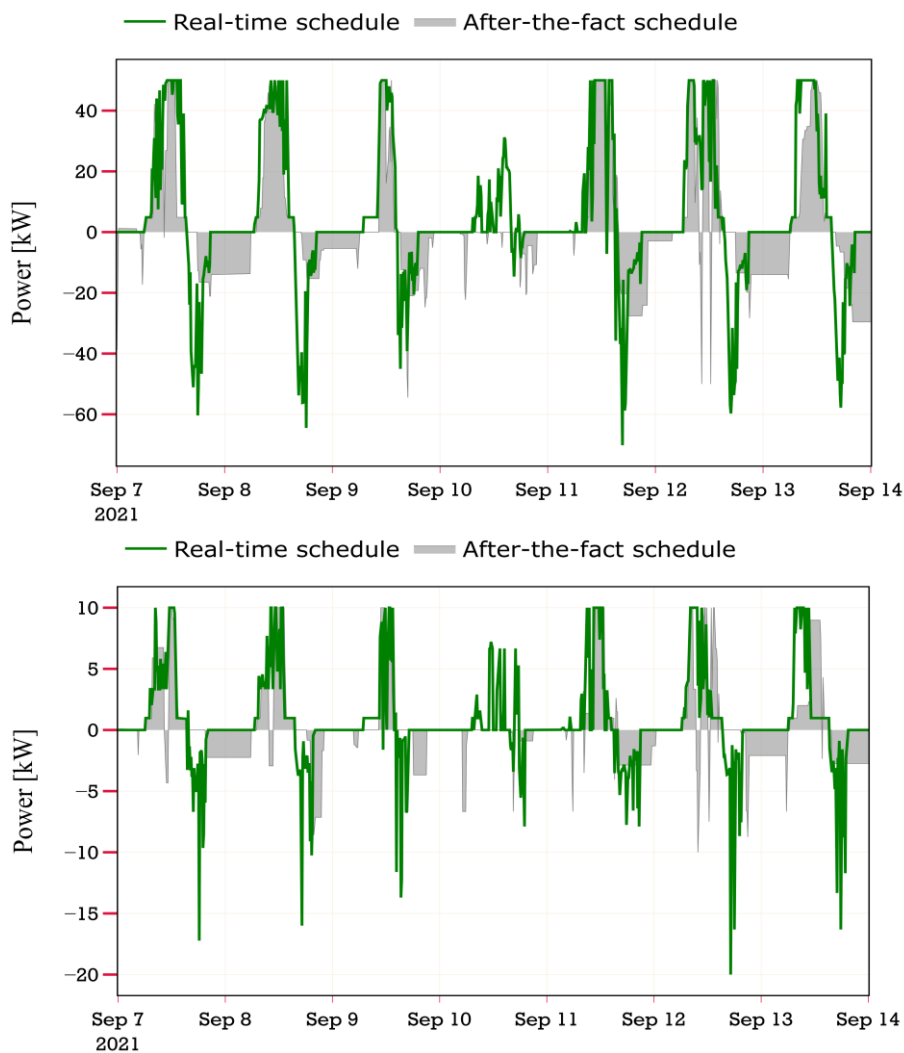


Figure 32. The real-time and after-the-fact schedules of batteries active power, top) the grid battery, bottom) the household battery.

As explained earlier in this section, the main objective of this work is the maximization of self-consumption from DSO's point of view. To evaluate the impact of proposed real-time control on self-consumption and peak load, the injected powers to the upper grid resulted from the real-time scheduling are compared with: i) the power injection resulted from the after-the-fact scheduling and ii) the exchanged power with upper grid without the batteries. Figure 33 shows the outputs of these two scenarios. The realized

patterns of injected power to upper grid resulted from the real-time and the after-the-fact schedules show the efficiency of the proposed control mechanism in terms of reducing positive and negative peaks. The proposed real-time control with real-time monitoring data has increased the self-consumption by %21.7. The after-the-fact scheduling without forecasting error increases the self-consumption by %28.3. Therefore, the self-consumption in the real-time control is %6.6 less than the optimal value calculated with the after-the-fact analysis. Moreover, the results show that implemented objective function shaves the peak load. On 9<sup>th</sup> September which the actual net-load is affected by high variation of PVs, %25.9 of the positive peak load is supplied by batteries and also, %32.0 of PVs generated power is stored in the batteries.

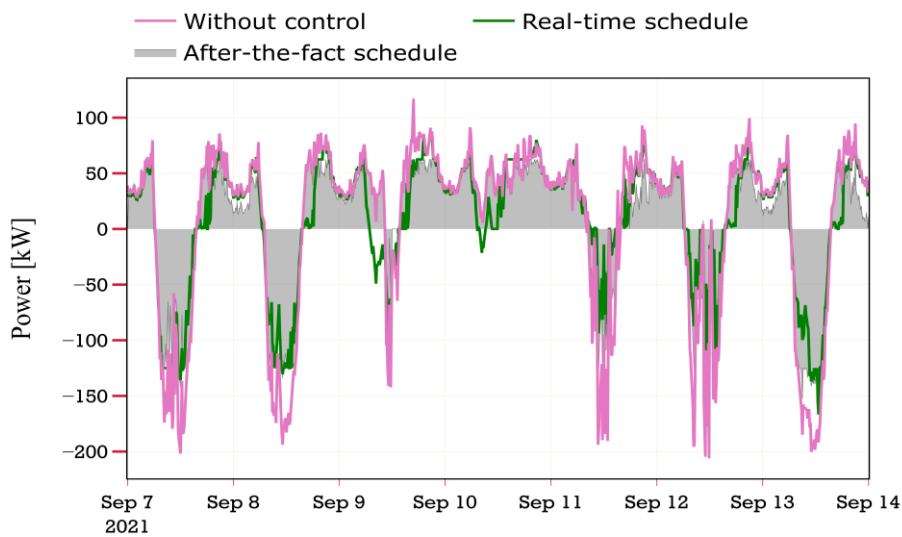


Figure 33. Injected power from upper grid.

In this work, a grid forecasting and control mechanism based on the real-time grid monitoring data is presented. The method integrates online data processing, rolling forecasting, and optimal control mechanism. The introduced rolling horizon forecasting method can predict the high-resolution net-load for the next 24-hours at every timeslot without the meteorology databases even in feeders with high PV production. The rolling forecasts of net-load accounts for the impact of behind-the-meter resources. Finally, the forecasted net-load is used for the optimal scheduling of battery energy storage systems. The performance of the proposed methodology is evaluated and compared with the results of after-the-fact analysis. Comparing the results show that the real-time methodology leads to near the optimal solution. Also, by testing on two consequent days we figured out that the batteries increase %23.1 usage of local renewable resources and DSO can benefit from the peak reduction of %29.1.

As the second stage of the work, the flexibilities of the PV inverters are integrated in the proposed control mechanism. It should be noted that the impact of a control setpoint on the voltages and power flows of the grid are considered through the sensitivity coefficients, as described in section 4. The developed control algorithm doesn't curtail PV productions and uses the available reactive power capacity of PV inverters for voltage control.